International Journal of Marine Energy 10 (2015) 17–38

Contents lists available at ScienceDirect

International Journal of Marine Energy

journal homepage: www.elsevier.com/locate/ijome

Fatigue reliability and calibration of fatigue design factors of wave energy converters

Simon Ambühl [*,1], Francesco Ferri [1], Jens Peter Kofoed [1], John Dalsgaard Sørensen [1]

Department of Civil Engineering, Aalborg University, Sofiendalsvej 11, 9200 Aalborg, Denmark

ARTICLE INFO

Article history:
Received 12 August 2014
Revised 8 January 2015
Accepted 8 January 2015
Available online 14 January 2015

Keywords:
Calibration
Fatigue design factor
Reliability
Stochastic model
Wave energy converter

ABSTRACT

Target reliability levels, which are chosen dependent on the consequences in case of structural collapse, are used in this paper to calibrate partial safety factors for structural details of wave energy converters (WECs). The consequences in case of structural failure are similar for WECs and offshore wind turbines (no fatalities, low environmental pollution). Therefore, it can be assumed that the target reliability levels for WEC applications can be overtaken from offshore wind turbine studies. The partial safety factors cannot be directly overtaken from offshore wind turbines because the load characteristics are different. WECs mainly focus on wave loads where for offshore wind turbine the wind loads are most dominating. Fatigue failure is an important failure mode for offshore structures. The scope of this paper is to present appropriate Fatigue Design Factors (*FDF*), which are also called Design Fatigue Factors (*DFF*), for steel substructures of WECs. A reliability-based approach is used and a probabilistic model including design and limit state equation is established. For modelling fatigue, the SN-curve approach as well as fracture mechanics are used. Furthermore, the influence of inspections is considered in order to extend and maintain a certain target safety level. This paper uses the Wavestar prototype located at Hanstholm (DK) as case study in order to calibrate *FDFs* for welded and bolted details in steel structures of an offshore bottom-fixed WEC with hydraulic floaters.

* Corresponding author.
E-mail addresses: sia@civil.aau.dk (S. Ambühl), ff@civil.aau.dk (F. Ferri), jpk@civil.aau.dk (J.P. Kofoed), jds@civil.aau.dk (J.D. Sørensen).
[1] Tel.: +45 30581879.

http://dx.doi.org/10.1016/j.ijome.2015.01.004
2214-1669/

1. Introduction

Wave energy converters (WECs) may become an important contributor of electricity from renewable energy sources in the future. Nowadays WECs exist on prototype level and are supposed to be further developed and improved.

Fatigue failures of offshore structures is a common failure mode. Fatigue failure often occurs in consequence of corrosion at welded structures or bolts. Background information about corrosion procedures in welds can be found in [1]. Due to the fact that failure consequences of a WEC lead to lower consequences (no risk of human life, low environmental pollution) compared with oil and gas platforms, WECs can be designed considering a lower safety level than oil and gas platforms. The consequences of failure of a WEC component can be assumed to be similar to failure consequences of a broken offshore wind turbine component. For offshore wind turbines, the dominating load is wind induced whereas for offshore platforms fatigue is mainly caused by wave loading [2]. Due to different safety levels as well as different dominating load characteristics and different control strategies compared with existing offshore structures, fatigue impact on WEC substructures need to be assessed and safety factors need to be calibrated.

The scope of this paper is to define appropriate partial safety factors (fatigue design factors) for steel substructures of WECs. In traditional deterministic designs, the amount of needed structural material is determined, among others, by the value of safety factors, which reflect the uncertainties related to design parameters and the required reliability level. Improved designs with consistent reliability levels can be obtained by probabilistic design methods. A reliability-based probabilistic approach, as used e.g. for offshore wind turbines [3], is used here where uncertainties related to loads, strengths and calculation methods are accounted for. A stochastic model for fatigue design has been established. Design and limit-state equations are developed based on a SN-curve approach. Palmgren–Miner rule with linear damage accumulation is used as recommended in most relevant standards, see e.g. [4] and [5]. Also a fracture mechanics approach is used for including different inspection strategies in order to maintain a given safety target level. Inspections can be used to extend the life-time as well as decrease the needed safety level due to better control of fatigue control growth [6]. Different inspection methods are compared as well as different inspection strategies based on an equidistant inspection plan or a risk-based inspection plan, where inspections are performed when the annual probability of failure exceeds the maximum acceptable annual probability of failure, are discussed.

An example is shown in the paper focusing on the Wavestar device which is located at Hanstholm (DK). This kind of device is an offshore bottom-fixed device which consists of floaters impelling a hydraulic system. The loads are determined using real measured wave states and an in-house hydrodynamic program (see [7] for more information) to estimate the loads.

In Section 2 general background information about probabilistic reliability assessments is given and Section 3 discusses acceptable reliability levels for fatigue failure of WECs. How fatigue can be modelled including no inspections (SN-curve approach) is shown in Sections 4.1 and 4.2 shows an approach when including inspections (Fracture mechanics). In Section 5, the Wavestar example is shown and resulting *FDF* values are shown. The conclusion from this article is given in Section 6.

2. Probabilistic reliability assessment

In practice, material characteristics of a structural detail (e.g. their yield stress), loads and environmental conditions contain uncertainties, which are not directly taken into account in a deterministic approach. Deterministic approaches only consider mean values of a certain parameter. Probabilistic reliability methods enable to model parameters as stochastic variables and take their uncertainties into account. There exist epistemic uncertainties which are related to limited data or limited knowledge about the behaviour of the system. Epistemic uncertainties can be reduced e.g. by increasing the knowledge and collecting more relevant data. Aleatory uncertainties are irreducible and account for physical uncertainties such as the fatigue strength. Epistemic and aleatory uncertainties need to be included in probabilistic reliability assessments.

Table 1
Examples of the reliability index β and the corresponding probability of failure P_F.

β	3.1	3.7	4.3	4.7	5.2
P_F	10^{-3}	10^{-4}	10^{-5}	10^{-6}	10^{-7}

For each failure mode of a structural component, it is possible to define a limit state function $g(t,\mathbf{X})$, where different uncertainties using stochastic variables $\mathbf{X} = \{X_1, X_2, \ldots\}$ are defined:

$$g(t,\mathbf{X}) = R(t) - S(t) = 0 \tag{1}$$

where $R(t)$ represents the resistance and $S(t)$ the loads at a certain time t. Failure occurs if the limit state equation is smaller than or equal to zero. The probability of failure, P_F, is equal to the probability that the limit state equation is smaller than or equal to zero:

$$P_F(t) = P(g(t,\mathbf{X}) \leqslant 0) \approx \Phi(-\beta(t)) \tag{2}$$

where $\Phi()$ is the standardized normal distribution and β the reliability index of the considered component's failure mode. The resulting limit state can be solved using FORM/SORM methods as well as simulation techniques (see e.g. [8,9]). FORM/SORM methods use a transformation in space where all stochastic variables become independent as well as standardized normal distributed. Therefore, the resulting reliability index β is assumed to be standardized normal distributed (see Eq. (2)). Table 1 shows examples of β values and the resulting probability of failure P_F. For time-dependent failure probabilities, $P_F(t)$, the annual probability of failure $\Delta P_F(t)$ given survival up to time t is obtained from:

$$\Delta P_F(t) = \frac{P_F(t) - P_F(t-\Delta t)}{\Delta t \cdot (1 - P_F(t))} \tag{3}$$

where Δt is equal to 1 year and $t > \Delta t$.

3. Acceptable reliability levels for fatigue failure of wave energy converters

Acceptable reliability levels depend on the application area as well as its impact in case of failure on human lives and resulting failure costs. Unmanned fixed offshore structures have according to [10] a minimal annual reliability index, $\Delta\beta$, in the interval 3.3–3.7. Ref. [11] groups the target annual reliability index for different costs of safety measures dependent on the consequences given failure of the structure, see Table 2. For wave energy converters it can be assumed that failure of the structure only has economic influences (no pollution and no fatalities). WECs are optimized such that the device is able to produce electricity at a competitive level compared with other devices. Therefore, costs are of importance and additional expenses should be prevented if possible. Due to the fact that WECs are most of the time unmanned, the relative costs for safety measures are high in order to prevent fatalities. Therefore, the resulting target annual reliability indices should be between 3.1 and 3.7 (see Table 2), which is in accordance with minimum acceptable reliability levels used for offshore wind turbines (OWTs) (see e.g. [12,13]).

Instead of focusing on the annual probability of failure, the probability of failure during the whole life-time can be considered. For fatigue limit states, Ref. [14] requires minimal cumulative reliability

Table 2
Target annual reliability index, $\Delta\beta$, according to [11].

Relative cost of safety measure	Consequences of failure		
	Minor	Moderate	Large
Large	3.1	3.3	3.7
Normal	3.7	4.2	4.4
Small	4.2	4.4	4.7

Table 3
Fatigue Design Factor (*FDF*) values proposed by [15].

FDF	Structural element
1	Internal structure, accessible and not welded directly to the submerged part
1	External structure, accessible for regular inspection and repair in dry and clean conditions
2	Internal structure, accessible and welded directly to the submerged part
2	External structure, not accessible for inspection and repair in dry and clean conditions
3	Non-accessible areas, areas not planned to be accessible for inspection and repair during operation

indices, β, between 2.3 and 3.1, dependent on the possibility of inspections. For OWTs, minimal cumulative reliability indices between 2.5 and 3.1 are considered (see [13]). This minimal cumulative reliability indices range is assumed to be transferrable from OWTs to WECs due to the same consequences in case of failure (no fatalities and low impact on environment).

The fatigue design criteria depends on whether the detail can be inspected and the location of the detail (influence of corrosion) as well as the resulting consequences, if the structural detail fails. Table 3 shows suggested *FDF* values proposed by DNV/Carbon Trust [15] for WEC steel structures based on failures with low consequences.

A more general overview is shown in Table 4 where different *FDF* values are compared from different standards used for different offshore applications. The *FDF* values for oil and gas structures are taken from [10]. Fatigue design factors used for OWTs are taken from [16] for bottom-fixed turbines and for floating wind turbines from [17]. Fatigue design factors in [17] including inspections assume inspection intervals between four and five years. The *FDF* values for WECs are taken from [15]. As expected the required *FDF* values for offshore oil and gas structures are higher than or equal for WECs and OWTs.

Due to the fact that WEC concepts/designs are still under development, different development stages, which lead to different uncertainty levels, should be considered when calibrating structural safety factors. There might be a prototype level, where high uncertainties related to the overall performance exist. The main purpose at that development stage is to show functionality of the device. In a developed stage, the target needs to be adjusted more towards cost-optimization and also decreasing the uncertainties due to gained knowledge. For different development stages different required *FDF* values result due to different uncertainty levels. The target reliability levels remain the same over the whole development process (see e.g. [18]).

Also the effect of using different materials (different SN-curves) as well as the effect of corrosion need to be considered in the design stage. There are design features (coating, cathodic protection or plate thickness allowance), which reduce the effect of corrosion. Whether or not such protection features are used should be defined and considered when defining *FDF* values.

In summary, the following points influence the calibration of *FDF* values:

- Consequences when structural detail fails,
- Considered inspection method and inspection plan,
- Location of considered detail (submerged, internal/external, effect of corrosion/cathodic protection), and

Table 4
Fatigue Design Factors (*FDFs*) required for different offshore industries and conditions (criticality and inspections) of external structures. OWT: offshore wind turbine; WEC: wave energy converter.

Failure critical detail	Inspections	Oil and gas [10]	OWT		WEC [15]
			Bottom-fixed [16]	Floating [17]	
Yes	No	10	3	6	3
Yes	Yes	5	2	3	2
No	No	5	2	3	2
No	Yes	2	1	2	1

- Development stage of system (developed, prototype) and the resulting uncertainties.

4. Reliability modelling of fatigue

This section focuses on approaches used to model fatigue reliability. When no inspections are considered, SN-curves together with Palmgren–Miner hypothesis, which assumes linear damage accumulation, can be used. SN-curves show the number of cycles with a certain stress amplitude leading to fatigue failure of the component. If inspections at a certain detail are performed, more information about the different stages of crack growth is needed. In this case fracture mechanics approaches, which are calibrated using SN-curves, can be used.

4.1. Reliability modelling of fatigue failure using SN-curves

In this section the SN approach, which is generally recommended for the design of offshore steel structures (see e.g. [10]), but also for (offshore) wind turbine designs (see e.g. [19–21]), is considered.

If a bilinear SN-curve, which has a slope change at $\Delta\sigma_D$ where the number of cycles to failure, N_D, is considered, the SN relation can be written as:

$$\begin{aligned} N &= K_1 S^{-m_1} \quad \text{for} \quad S \geqslant \Delta\sigma_D(N_D) \\ N &= K_2 S^{-m_2} \quad \text{for} \quad S < \Delta\sigma_D(N_D) \end{aligned} \tag{4}$$

where N is equal the number of cycle leading to failure for a given stress amplitude S. The parameters K_1, K_2, m_1 as well as m_2 are SN-curve parameters.

It is assumed that the stress range $\Delta\sigma = \Delta Q/z$ can be obtained on basis of load effect range ΔQ (e.g. normal force) and the design parameter z (e.g. cross-sectional area). Further, it is assumed that the total number of stress ranges for a given fatigue critical detail can be grouped into groups/intervals of stress amplitudes such that the number of stress ranges in group i is n_i per year. $(\Delta Q_i, n_i)$ is obtained by rainflow counting (see e.g. [22]).

The code-based design equation, which is needed to calibrate the design parameter z, using Palmgren–Miner rule can be written as:

$$G = 1 - \underbrace{\sum_i \sum_j \sum_{k_1} \frac{T_{FAT} n_{ijk_1}}{K_1^c} s_{ijk_1}^{m_1} P(H_{S_i}, T_{P_j})}_{s_{ijk_1} \geqslant \Delta\sigma_D} - \underbrace{\sum_i \sum_j \sum_{k_2} \frac{T_{FAT} n_{ijk_2}}{K_2^c} s_{ijk_2}^{m_2} P(H_{S_i}, T_{P_j})}_{s_{ijk_2} < \Delta\sigma_D} = 0 \tag{5}$$

where K_1^c and K_2^c are the characteristic values of K_1 and K_2, n_{ijk} is the number of cycles per year of stress range k given a certain wave state (significant wave height H_{S_i} and peak period T_{P_j}), $s_{ijk} = \Delta Q_{ijk}/z$ is the stress range k given H_{S_i} and T_{P_j}, $P(H_{S_i}, T_{P_j})$ is the probability of occurrence of a certain wave state given by H_{S_i} and T_{P_j}. The fatigue life, T_{FAT}, includes the fatigue design parameter, FDF, for fatigue design:

$$FDF = \frac{T_{FAT}}{T_L} \tag{6}$$

where T_L is equal to the life-time of the device. The fatigue design factor is calibrated in this paper. Note that for a linear SN-curve with slope m, the partial safety factors for fatigue load, γ_f, and fatigue strength, γ_m, show the following relation:

$$FDF = \left(\gamma_f \gamma_m\right)^m \tag{7}$$

The probability of failure and its corresponding reliability index can be calculated using the design parameter z determined with Eq. (5) in a limit-state equation. The considered limit state equation is similar to the design equation:

$$g(t) = \Delta - \underbrace{\sum_i \sum_j \sum_{k_1} \frac{t n_{ijk_1}}{K_1} s_{ijk_1}^{m_1} P(H_{S_i}, T_{P_j})}_{s_{ijk_1} \geqslant \Delta\sigma_D} - \underbrace{\sum_i \sum_j \sum_{k_2} \frac{t n_{ijk_2}}{K_2} s_{ijk_2}^{m_2} P(H_{S_i}, T_{P_j})}_{s_{ijk_2} < \Delta\sigma_D} = 0 \tag{8}$$

where t indicates the time ($0 \leqslant t \leqslant T_L$), K_1 and K_2 are stochastic SN-curve specific variables, Δ represents the model uncertainty related to Palmgren–Miner rule for linear damage accumulation, $s_{ijk} = X_M X_{SCF} \Delta Q_{ijk}/z$ is the stress range ijk given H_{S_i} and T_{P_j}. The model uncertainty X_M models the uncertainties related to estimation of load effect ranges including uncertainties of wave climate and wave load calculation. The stress concentration factor uncertainty (X_{SCF}) models the uncertainty related to the geometry and location of the welded detail. Inter-annual variations of the load characteristics may also be considered.

4.2. Reliability taking into account inspections

For oil and gas offshore structures, inspections of fatigue critical details are performed in order to maintain a sufficient reliability level. This can also be adapted for fatigue critical components of WECs. But the resulting costs of inspections and possible repairs in case of detected cracks should be compensated by lower investment costs (lower *FDF* values).

There are different ways to decide when inspections should be performed. Fig. 1 shows two different inspection planning strategies. The simplest inspection planning strategy considers fixed inspection intervals (Fig. 1A). Another inspection plan strategy (Fig. 1B) focuses more on the requirement that the annual probability of failure, $\Delta P_F(t)$, in all years has to satisfy the reliability constraint (reliability-based inspection planning):

$$\Delta P_F(t) \leqslant \Delta P_{F,MAX} \tag{9}$$

where $\Delta P_{F,MAX}$ is the maximum acceptable probability of failure. When the annual probability of failure exceeds, inspections are performed. It is assumed that if cracks are detected, they have to be repaired. This inspection strategy results in non-equidistant time intervals and typically increased time intervals between inspections compared with equidistant inspection intervals.

When risk-based inspection is taken into account, a decision rule needs to be specified what should be done when a crack is detected. Furthermore, costs related to the repair, inspection and discounting need to be known and weather effects/windows will impact planned inspection intervals. The theoretical basis for risk-based inspection and maintenance planning for fatigue critical details for offshore steel substructure applications is described e.g. in [2,23].

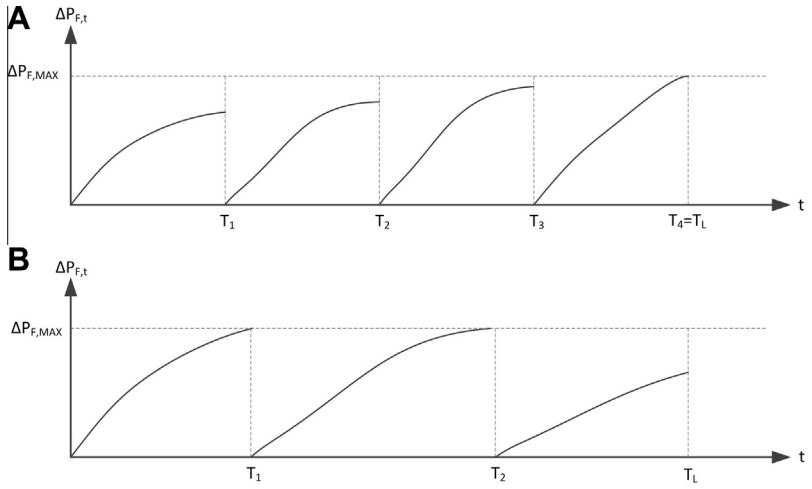

Fig. 1. Illustration of different inspection plans. (A): Equidistant inspections – Inspection plan with equidistant inspection intervals; (B): Risk-based inspections – Inspection plan where inspections are performed when the annual probability of failure ($\Delta P_{F,t}$) exceeds the maximum acceptable probability of failure ($\Delta P_{F,MAX}$).

The impact of inspections on structural reliability of a certain substructure depends on the inspection quality. The quality of the inspection itself can be described using a so-called probability of detection (P_D) curve, which is a function of the crack length c. Ref. [24] describes a P_D curve for non-destructive examination (NDE) techniques in the following way:

$$P_D(c) = 1 - \frac{1}{1 + \left(\frac{c}{x_0}\right)^b} \tag{10}$$

where b and x_0 are parameters dependent on the used inspection technique as well as whether the inspection is performed above the water surface or under water. Table 5 gives P_D curve parameters (see Eq. (10)) for Eddy current as well as Magnetic Particle Inspection (MPI) techniques.

A P_D curve can also be described dependent on the expected smallest detectable crack length, λ, using e.g. an exponential model (see e.g. [25]):

$$P_D(c) = 1 - \exp\left(-\frac{c}{\lambda}\right) \tag{11}$$

The P_D curve presented in Eq. (11) can be used to model e.g. inspection reliability when visual inspection is performed.

When inspection of a crack is performed at a certain time T_{insp} either detection or no detection occurs. The outcome of an inspection during service-life can be used to update the reliability of the considered detail as well as its inspection plan. If an inspection is performed at T_{insp} and no crack has been detected, the probability of failure can be updated to P_F^U:

$$P_F^U(t|\text{no crack detection at } T_{insp}) = P\big(g(t) \leqslant 0 | h(T_{insp} > 0)\big), \quad t > T_{insp} \tag{12}$$

where $h(t)$ is the limit state modelling crack detection. If an inspection technique is related to the crack length $c(t)$ at time t, then $h(t)$ can be written as:

$$h(t) = c_d - c(t) \tag{13}$$

where c_d is the smallest detectable crack length, which can be modelled as a stochastic variable with a cumulative distribution function equal to the P_D curve:

$$F_{c_d}(c) = P_D(c) \tag{14}$$

When including inspections of a fatigue critical detail in fatigue assessments, fracture mechanical (FM) approaches can be used to model fatigue failure. Fracture mechanics model can be calibrated by fitting the FM model assuming no inspection actions to a probabilistic SN approach with Palmgren–Miner rule and linear damage accumulation. The FM approach (without inspections) and the SN approach should give the same reliability levels. The fatigue life may be represented by crack initiation time and crack propagation time. Therefore, the number of stress cycles to failures, N, can be written as:

$$N = N_I + N_P \tag{15}$$

where N_I is the number of cycles needed before a crack starts to propagate and N_P indicates the number of cycles from initiation to crack through. Cracks can be divided into fabrication cracks, which should be detected by fabrication control and initial inspections, and growing fatigue cracks, which

Table 5
P_D curve parameters (see Eq. (10)) for different inspection technologies. [24].

Inspection method	x_0	b
MPI underwater	2.950 mm	0.905
MPI above water, ground test surface	4.030 mm	1.297
MPI above water, not ground test surface	8.325 mm	0.785
Eddy current	12.28 mm	1.790

should be detected by inspections during life-time. Fabrication inspections are not considered in the following.

It is assumed that the crack can be modelled by an approximated 2-dimensional semi-elliptical crack. The definition of crack length c, crack depth a, thickness T and main load direction is shown in Fig. 2.

The crack growth rate per load cycle can be described using the following power law [26]:

$$\frac{da}{dN} = C(\Delta K(a))^m, \quad a(0) = a_0 \tag{16}$$

where C and m are experimentally determined parameters and a_0 is the initial crack depth. The stress intensity range ΔK can be determined from:

$$\Delta K(a) = Y \Delta\sigma_e \sqrt{\pi a} \tag{17}$$

where Y is a geometry function and $\Delta\sigma_e$ is the equivalent stress range determined from:

$$\Delta\sigma_e = \left(\frac{1}{n}\sum_{i=1}^{n} \Delta\sigma_i^m\right)^{1/m} \tag{18}$$

where n is the number of considered stress cycles and $\Delta\sigma_i$ the stress amplitude of cycle i. In general two coupled differential equations (one for crack length c and one for crack depth a) can be formulated. These equations can be formulated based on e.g. [27]. Sometimes the crude simplification is made that $2c/a$ is a constant (e.g. = 5). Another simplification is to use:

$$\frac{a}{2c} = f\left(\frac{a}{T}\right) \tag{19}$$

where the depth-length ratio $(a/2c)$ can be calculated as function of the relative crack depth a/T. The depth-length ratio, $(a/2c)$, depends on the geometry as well as the loading conditions and can be found e.g. in [27].

The stress range, $\Delta\sigma$, includes uncertainties related to load modelling (X_M) as well as stress concentration factor (X_{SCF}):

$$\Delta\sigma = X_M X_{SCF} Y \Delta\sigma_e \tag{20}$$

The limit state can be written in terms of the number of cycles, N, leading to failure:

$$g(\mathbf{X}) = N - nt \tag{21}$$

where t is the time (in years) between 0 and the life-time, T_L, and n the number of cycles per year. Equivalently, the limit-state can be written in terms of crack depth:

$$g(\mathbf{X}) = a_c - a(t) \tag{22}$$

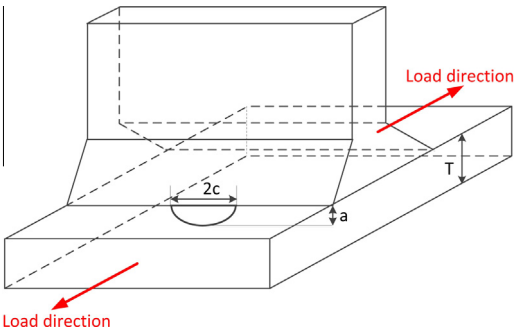

Fig. 2. Definition of crack parameters for a 2-dimensional semi-elliptical crack. 2 c: crack length; a: crack depth; T: thickness plate.

where $a(t)$ is the crack depth dependent on time t and the a_c the critical depth, which typically is the thickness T.

5. Example: Wavestar WEC

In this example the Wavestar prototype device (see Fig. 3) is considered. This device is placed near Hanstholm at the Danish Westcoast of the North Sea. The prototype consists of two floaters, four piles with a gravity-based foundation as well as a platform which connects the piles and the floater and on which the mechanical and electrical components are placed. The floaters, which are excited by passing waves, drive a hydraulic cycle which impels a turbine and a generator. The Wavestar prototype has a nominal capacity of 110 kW and has been feeding electricity into the grid since 2010 [28].

Near the prototype there are wave states measurements from a buoy available over six years and provided by [29]. The buoy measured the significant wave height H_S and the peak period T_P with time intervals of 3 h. The resulting scatter diagram with the probability of occurrence is shown in Table 6. For each sea state described in Table 6, 30 h of wave elevation time-series are used as input for the numerical simulation tool, which calculates the loads onto the structure for a given control strategy as well as surface wave elevation time-series. Here, two control strategies are considered. A simple P-controller as well as the active PI-control strategy, which is known as spring-damper controller, are used. The P-controller is a passive damper control system where the control force is proportional to the velocity of the body velocity. The PI-controller uses compared to the P-controller an additional term for the control force, which is proportional to the position of the body. More information about the controllers and their implementations are available in [7]. According to [28] and [30] is the operational range, where the Wavestar device is producing electricity 0.5 m $\leqslant H_S \leqslant$ 3 m. For other significant wave heights, the floater is taken out of the water. The same wave-state range is considered for calculating the design parameter z (see Eq. (5)) as well as the probability of structural failure from the limit state function (see Eq. (8)). Different wave state ranges will impact the design parameter but the differences of *FDF* values for a given target reliability level is of minor importance because the same load spectra are used for the deterministic design as well as the probabilistic approach.

Two welds and one bolted connection are considered here for calibration of Fatigue Design Factors (*FDF*). For all three details, the load at its specific location is considered. These fatigue critical details are investigated here, because their structural failure will release the floater arm and the platform. Fig. 4 shows the locations of the considered three details. Their different SN-curves are taken from [4] and can be seen in Table 10.

Fig. 3. Point absorber Wavestar prototype located near Hanstholm (DK) with two 5 m floaters and a floater arm length of 10 m. The main dimensions are: 32 m × 17 m × 6.5 m (L × W × H).

Table 6
Relative occurrence of different wave states from 6 years buoy measurements ($[H_S] = m$, $[T_P] = s$) [29].

H_S/T_P	0.5	1.5	2.5	3.5	4.5	5.5	6.5	7.5
0.25	–	–	–	0.04	0.04	0.02	0.01	–
0.75	–	–	–	0.07	0.17	0.11	0.05	0.01
1.25	–	–	–	–	0.06	0.11	0.05	0.01
1.75	–	–	–	–	–	0.06	0.05	0.02
2.25	–	–	–	–	–	0.01	0.05	0.02
2.75	–	–	–	–	–	–	0.01	0.02
3.25	–	–	–	–	–	–	–	0.01

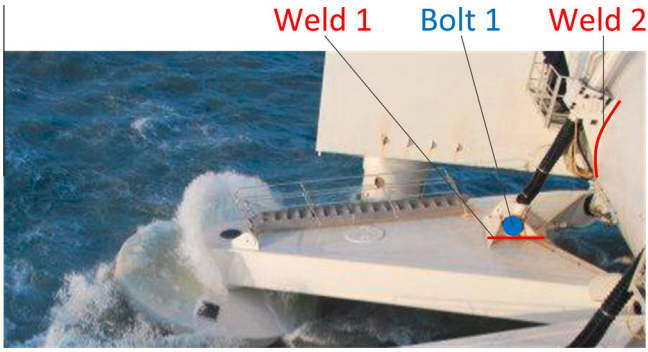

Fig. 4. Locations at Wavestar WEC where calibration of *FDF* is performed.

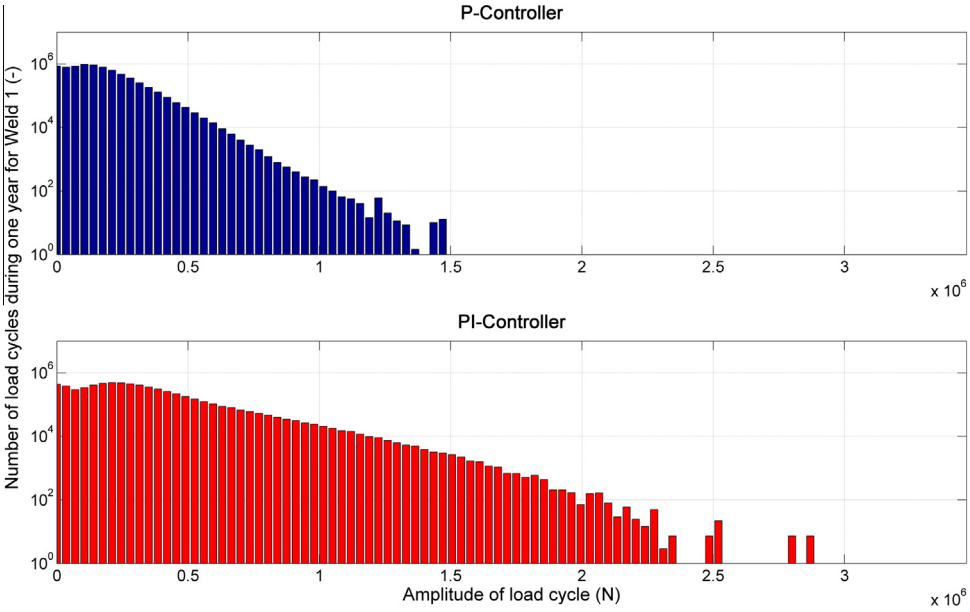

Fig. 5. Expected number of load cycles during one year at Weld 1 for P and PI control strategy.

The expected number of cycles during one year resulting from rainflow counting for the P-controller as well as PI-controller is shown in Fig. 5 for Weld 1. The PI-controller leads to larger amounts of loads with large amplitude whereas the P-controller has more cycles with small load amplitudes.

Larger fatigue load amplitude ranges for PI-controller compared with the P control strategy are also observed for the two other locations. The total annual number of load cycles is equal to 7.5×10^6 for the P-controller and 6.6×10^6 for the PI-controller. The PI-controller enables to harvest more energy from the waves. With the active PI control strategy 117.3 MWh are harvested per year from the waves, whereas for the simple P-controller, the absorbed annual energy is equal to 57.6 MWh. On the other hand lead the PI-controller to larger loads compared when using the P-controller. At Weld 1 for example the equivalent force is 2.1 times larger when using the PI-controller instead of the simpler P-controller strategy. Which control strategy is best, can be evaluated by an overall cost–benefit consideration.

5.1. Assessment of model uncertainty

A lab-scaled floater with a diameter of 0.25 m is used to specify the model uncertainty, X_{LM}, which is related to wave load calculations and rainflow counting. For estimating the model uncertainty, the numerical simulation is also performed at the down-scaled wave state and with the same controller configuration as used in the experimental setup. The lab-scaled floater compared with the prototype floater is down-scaled with a factor 20 using Froude law. The wave state conditions where the lab-experiments are performed, are up-scaled equal to the wave state (H_S = 0.75 m and T_P = 4.5 s), where the probability of occurrence is largest (see Table 6). The JONSWAP spectrum with a peak enhancement factor equal to 3.3 is used.

The experimental setup measures the loads with a load cell in power take-off (hydraulic cylinder) direction. This load is decomposed in normal and tangential load from a geometrical consideration taking the motion of the floater into account. The instantaneous location of the floater is determined with a laser measuring the instantaneous length of the hydraulic cylinder. In order to reproduce the same wave time-series in the experiment and the simulation tool, the same experiment was performed twice: with the floater activated and without the floater but a wave gauge at the position of the floater. The results from the wave gauge were used as input (wave elevation time-series) for the numerical simulation tool. The same wave elevation time-series enable to estimate the model uncertainty for fatigue load spectra. Further information about the experimental setup can be found in [31]. The model uncertainty, X_{LM}, represents ratio between the load amplitudes resulting from the experiments (ΔL_{exp}) and the simulations (ΔL_{num}):

$$X_{LM} = \frac{\Delta L_{exp}}{\Delta L_{num}} \tag{23}$$

In order to weight the load amplitude size on the structural damage, the load ranges are weighted in the following way, as shown for the experimental time-series:

$$\Delta L_{exp} = \left(\frac{1}{N_{exp}} \sum_{i=1}^{N_{exp}} (\Delta L_{exp,i})^m \right)^{1/m} \tag{24}$$

where N_{exp} is equal the number of cycles considered during a certain time interval and m is equal to the slope in a linear SN-curve. To estimate the model uncertainty, the considered total time-series length is divided into a certain number of time intervals (e.g. 20), where for each time interval the ratio shown in Eq. (23) is calculated. The resulting model uncertainty is assumed to be Lognormal distributed [11].

Table 7 shows the resulting model uncertainty, X_{LM}, for different SN-curve slopes (m-values) and two control strategies. All three different locations show the same model uncertainties for a given m-value and control system. A larger SN-curve slope leads to larger model uncertainties. The numerical simulations using a PI control algorithm slightly underestimates the loads. The PI-controller has larger model uncertainties compared with the P-controller. In general, the estimated uncertainties are without importance (*COV* very low). Fig. 6 shows part of a load time-series for Weld 1 from experiments and simulations using a PI control system.

Table 7
Resulting model uncertainty X_{LM} for different m-values (SN-slope) as well as two different control systems. μ: mean value; COV: coefficient of variation.

Controller	Statistics	$m = 3$	$m = 5$
P	μ	1.00	1.00
	COV	0.01	0.02
PI	μ	1.02	1.03
	COV	0.01	0.02

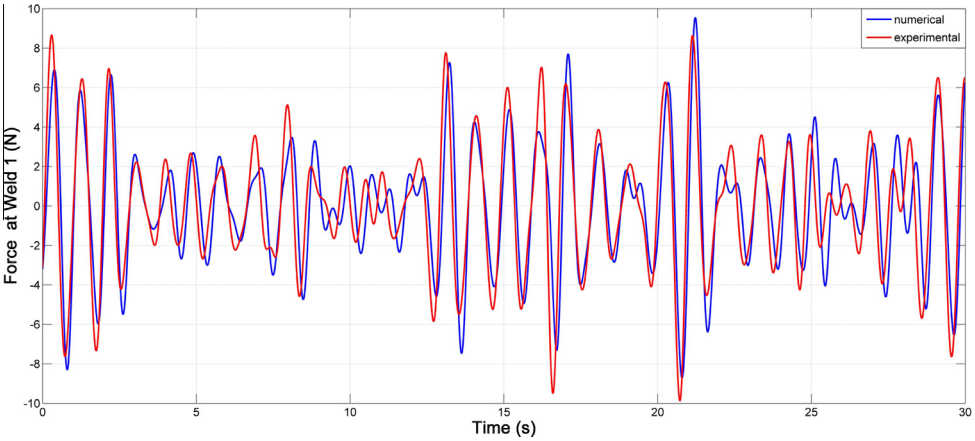

Fig. 6. Example of lab-scaled load time-series ($H_S = 0.0375$ m and $T_P = 1$ s) for Weld 1 location using PI control strategy.

5.2. Required FDF with no inspections

In order to model fatigue without inspection consideration, the SN-approach is used. The uncertainties resulting from the wave load modelling are taken from Section 5.1. For the *COV* value related to the uncertainty about stress concentrations (X_{SCF}), a parameter study is performed. The uncertainty of the stress concentration factor (*SCF*) depends on the level of the used model and the overall analysis complexity. Table 8, which is partly based on [12], shows an example when different *SCF* uncertainties are used. *COV* values for *SCF* are considered to be in general between 0.0 and 0.2. When using FEM methods as well as experimentally validated loads at the location of interest, the uncertainty about *SCF* can be decreased compared with using simple *SCF* parametric equations. When validating modelled loads with experimental data at the location of interest, uncertainties about *SCF* are partly included in the measurement uncertainties.

The *COV* values of the model uncertainties associated with Palmgren–Miner Rule, COV_Δ and the standard deviation for $\log K_1$ and $\log K_2$ follow the recommendations in [4]. It is noted that uncertainties related to Δ as well as $\log K_i$ should be modelled carefully, due to the fact that their influence can be significant. The values $\log K_1$ and $\log K_2$ are assumed to be fully correlated. The general model uncertainty X_M used in Eq. (8) is further divided into different model uncertainties:

$$X_M = X_{Wave} X_{LM} \tag{25}$$

where X_{Wave} is the effect of uncertainties related with site assessment of the considered location and X_{LM} (see Section 5.1) represents the modelling uncertainty related to wave load calculation, fatigue loads as well as rainflow counting. Table 9 shows an example of site assessment uncertainties of wave conditions due to limited wave data and considered wave directions applicable for the Wavestar

Table 8
Examples of different stress concentration (*SCF*) uncertainties (COV_{SCF}) dependent on the level of load calculations method and complexity of fatigue detail. Values for X_{SCF} partly based on [12].

X_{SCF}	Fatigue critical detail
0.00	Use of FEM tools at the considered location for statistically determinate systems with simple fatigue critical details
0.05	Use of FEM tools at the considered location for statistically determinate systems with complex fatigue critical details
0.10	Use of FEM tools at the considered location for statistically in-determinate systems with complex fatigue critical details
0.15	Use of SCF parametric equations for simple fatigue critical details
0.20	Use of SCF parametric equations for complex fatigue critical details

Table 9
Example of site assessment uncertainty, X_{Wave}, for wave conditions based on available (limited) wave data and wave direction influence. The presented uncertainty values are partly transferred from wind data uncertainties used for wind turbines, see [32].

COV_{Wave}	Limited wave data and wave direction influence
0.05	More than 2 years of wave data available and direction of incoming waves considered in load calculations
0.10	More than 2 years of wave data available and direction of incoming waves not considered in load calculations
0.15	At least 1 year of wave data available and direction of incoming waves considered in load calculations
0.20	Less than 1 year of wave data available and direction of incoming waves considered in load calculations
0.25	Less than 1 year of wave data available and direction of incoming waves not considered in load calculations

device. The data in Table 9 is partly based on wind data uncertainties used for wind turbines, see [32]. The more data one has available, the lower the statistical uncertainty due to limited dataset length. Smaller datasets might not cover the whole load spectrum and lead therefore to larger uncertainties compared with large datasets. Another uncertainty source is the incoming wave direction enabling or disabling generation of wave incoming dependent load spectra. The wave modelling uncertainties, X_{Wave}, may be different for other WECs due to the fact that some WECs can weathervane and their impact on the directional influences may be of minor importance.

The stochastic model used for reliability modelling of fatigue details is shown in Table 10. The stochastic model in general assumes no gross fabrication defects.

Table 10
Uncertainty modelling used for reliability analysis with SN approach. Std. dev.: Standard deviation, D: Deterministic, N: Normal, LN: Lognormal.

Variable	Meaning	Dist.	Expected values	Std. dev.	Char. value	Source
Δ	Unc. Resistance	LN	1	0.3	1	[4]
X_{SCF}	Unc. SCF	LN	1	0.00/0.05/ 0.1/0.15/0.2	1	Table 8
X_{LM}	Unc. load model	LN	1	Section 5.1	1	
X_{Wave}	Unc. site assessment	LN	1	0.1	1	Table 9
Weld 1 - In Air - Detail 'F'						
$\log K_1$	SN curve parameter	N	12.255	0.2	11.855	[4]
$\log K_2$	SN curve parameter	N	15.491	0.2	15.091	[4]
m_1	SN curve parameter	D	3		3	[4]
m_2	SN curve parameter	D	5		5	[4]
Weld 2 - In Air - Detail 'E'						
$\log K_1$	SN curve parameter	LN	12.410	0.2	12.010	[4]
$\log K_2$	SN curve parameter	N	15.735	0.2	15.350	[4]
m_1	SN curve parameter	D	3		3	[4]
m_2	SN curve parameter	D	5		5	[4]
Bolt 1						
$\log K_1$	SN curve parameter	N	16.701	0.2	16.301	[4]
$\log K_2$	–	–	–		–	[4]
m_1	SN curve parameter	D	5		5	[4]
m_2	–	–	–		–	[4]

Table 11
Resulting annual reliability indices ($\Delta\beta$) for Weld 1 using two different control systems (P and PI algorithm), different model uncertainties (related to *m*-value, see Table 7) and different fatigue design factors (*FDF*). COV_{SCF} is equal to 0.1.

Control system	*m*-value	FDF				
		1	2	3	5	10
P	3	2.2	2.7	3.1	3.5	4.2
	5	2.2	2.7	3.1	3.5	4.2
PI	3	2.2	2.7	3.0	3.5	4.1
	5	2.2	2.6	3.0	3.4	4.1

Table 12
Required *FDF* values for Weld 1 dependent on *SCF* uncertainty and minimal annual reliability $\Delta\beta$ using two different control algorithms (P and PI control systems).

Control system	$\Delta\beta$	COV_{SCF}				
		0	0.05	0.1	0.15	0.2
P	3.1	2.5	2.7	3.2	4.1	5.6
	3.7	4.3	4.7	6.1	9.1	>10
PI	3.1	2.6	2.8	3.3	4.3	6.0
	3.7	4.5	4.8	6.5	9.5	>10

An example of resulting annual reliability levels of Weld 1 for given *FDF* values is shown in Table 11. In general, the PI control system leads to slightly smaller $\Delta\beta$ values for a given *FDF* value due to fact that the model uncertainty X_{LM} is larger for the PI control system compared with the simple passive damping system (P-controller). The difference of $\Delta\beta$ values for a given control strategy and *FDF* value, but different *m*-values (SN-curve slope) is negligible.

5.2.1. Influence of stress concentration factor (SCF) uncertainty

As shown in Table 8 depends the uncertainty about stress concentration on the level of complexity and used stress modelling tools. Here, the impact of *SCF* uncertainty on calibration of *FDF* values is discussed. Table 12 shows *FDF* calibration results of Weld 1 for minimal annual reliability indices of 3.1 and 3.7, respectively. Two different control strategies are considered and the stochastic model shown in Table 10 is used. *FDF* calibration results for Weld 2 and Bolt 1 are shown in Tables 13 and 14, respectively. Different *FDF* calibration results for the three different details at a given COV_{SCF} value occur due to the fact that different load spectra and different SN-curves are considered. In general, increased *SCF* uncertainty leads to larger required *FDF* values for a given minimal annual reliability index $\Delta\beta$. The largest *FDF* values result for Bolt 1. The differences at a given COV_{SCF} value in required *FDF* values for Weld 1 and Weld 2 are almost negligible. For a given *SCF* uncertainty level and a certain control system, different *FDF* values for the three locations occur due to different considered SN-curves.

Calibration of *FDF* can also be done dependent on the cumulative reliability index β. Tables 15–17 show resulting *FDF* values calibrated for Weld 1, Weld 2 and Bolt 1 requiring a cumulative reliability index equal to 2.5 and 3.1.

Table 13
Required *FDF* values for Weld 2 dependent on *SCF* uncertainty and minimal annual reliability $\Delta\beta$ using two different control algorithms (P and PI control systems).

Control system	$\Delta\beta$	COV_{SCF}				
		0	0.05	0.1	0.15	0.2
P	3.1	2.5	2.6	3.1	4.0	5.4
	3.7	4.2	4.6	6.0	8.8	>10
PI	3.1	2.6	2.7	3.2	4.1	5.3
	3.7	4.3	4.7	6.0	8.6	>10

Table 14
Required *FDF* values for Bolt 1 dependent on *SCF* uncertainty and minimal annual reliability $\Delta\beta$ using two different control algorithms (P and PI control systems).

Control system	$\Delta\beta$	COV_{SCF}				
		0	0.05	0.1	0.15	0.2
P	3.1	2.7	3.0	3.7	5.0	6.9
	3.7	4.8	5.3	7.3	>10	>10
PI	3.1	2.5	2.8	3.5	4.9	7.0
	3.7	4.0	4.6	6.5	>10	>10

Table 15
Required *FDF* values for Weld 1 dependent on *SCF* uncertainty and minimal cumulative reliability β using two different control algorithms (P and PI control systems).

Control system	β	COV_{SCF}				
		0	0.05	0.1	0.15	0.2
P	2.5	2.3	2.5	3.1	4.2	6.1
	3.1	3.6	3.9	5.3	7.9	>10
PI	2.5	2.4	2.6	3.1	4.2	6.1
	3.1	3.8	4.1	5.5	7.9	>10

Table 16
Required *FDF* values for Weld 2 dependent on *SCF* uncertainty and minimal cumulative reliability β using two different control algorithms (P and PI control systems).

Control system	β	COV_{SCF}				
		0	0.05	0.1	0.15	0.2
P	2.5	2.3	2.5	3.0	4.1	5.8
	3.1	3.5	3.9	5.2	7.5	>10
PI	2.5	2.4	2.5	3.1	4.0	5.6
	3.1	3.7	4.0	5.0	7.3	>10

Table 17
Required *FDF* values for Bolt 1 dependent on *SCF* uncertainty and minimal cumulative reliability β using two different control algorithms (P and PI control systems).

Control system	β	COV_{SCF}				
		0	0.05	0.1	0.15	0.2
P	2.5	2.6	2.8	3.7	5.3	8.0
	3.1	4.0	4.6	6.3	9.9	>10
PI	2.5	2.3	2.6	3.5	5.1	7.9
	3.1	3.4	3.9	5.6	9.3	>10

5.2.2. Influence of SN-curve uncertainty

According to [4] is a standard deviation of the SN-curve, which is reflected in the uncertainty of the *K*-parameter, suggested to be equal to 0.2. Due to more experiments or detail-specific SN-curves, its uncertainty can be reduced. Here, a reduction of σ_K from 0.2 to 0.15 is investigated for Weld 1. The SN-curve model used for $\sigma_K = 0.15$ is shown in Table 18.

The resulting required *FDF* values considering different SN-curve uncertainties (different σ_K values) are shown in Table 19 for annual minimal reliability indices and for minimal cumulative reliability indices. The results in Table 19 consider the same characteristic values of the *K*-parameter, which

Table 18
SN-curve from [4] for Weld 1 with reduced *K*-parameter uncertainty, which reflects the uncertainty of the SN-curve. Std. dev.: Standard deviation, D: Deterministic, N: Normal.

Variable	Meaning	Dist.	Expected values	Std. dev.	Char. value
		Weld 1 - In Air - Detail 'F'			
$\log K_1$	SN curve parameter	N	12.155	0.15	11.855
$\log K_2$	SN curve parameter	N	15.391	0.15	15.091
m_1	SN curve parameter	D	3		3
m_2	SN curve parameter	D	5		5

are used for the deterministic design of Weld 1, for different σ_k values. But different mean values of the stochastic model are considered for different σ_K values. Smaller *K* uncertainties lead for the considered case to larger required *FDF* values due to the fact that the difference between the characteristic value and the expected mean value of the stochastic model becomes smaller.

5.2.3. Influence of environmental conditions

Different WECs are operating in air and others (or part of a WEC) are operating in water. Here the impact of environmental conditions is assessed by using different SN-curves for Weld 1. The representative SN-curves are taken from [4] where a 'F'-detail is considered with the following respect to operation in water:

- Fatigue critical detail in marine critical conditions with cathodic protection, and
- Fatigue detail in water with subject to free corrosion.

The values used for the two SN-curves assuming operation below the water surface are shown in Table 20.

Fig. 7 shows an example of the resulting minimal annual reliability index $\Delta\beta$ for different *FDF* values and SN-curves. Table 21 shows the required *FDF* values for Weld 1 for minimal annual reliability indices equal to 3.1 and 3.7 as well as for minimal cumulative reliability indices equal to 2.5 and 3.1 using P as well as PI control algorithms. The uncertainty for stress concentration factor (COV_{SCF}) is assumed to be equal to 0.1. The results from operation 'in air' and 'cathodic protection' show similar required *FDF* values. Lowest *FDF* values are reached for the linear SN-curve assuming free corrosion below water surface.

Also of importance when comparing different SN-curves is the ratio of fatigue damage between the two curves with *m* equals to 3 and 5, respectively. The relative fatigue damage ratio, D_{rel}, is considered here according to:

Table 19
Required *FDF* values for Weld 1 for different minimal annual reliability indices $\Delta\beta$ and minimal cumulative reliability indices β with different SN-curve uncertainties using two different control algorithms (P and PI control systems). Different SN-curve uncertainties are presented by different standard deviations (σ_K) of the SN-curve parameter *K*.

Control system	$\Delta\beta$	σ_K	
		0.15	0.20
P	3.1	3.6	3.2
	3.7	6.5	6.1
PI	3.1	3.7	3.3
	3.7	6.8	6.5
Control system	β	σ_K	
		0.15	0.20
P	2.5	3.4	3.1
	3.1	5.5	5.3
PI	2.5	3.5	3.1
	3.1	5.6	5.5

Table 20
SN-curves from [4] for structural parts below water surface. Std. dev.: Standard deviation, D: Deterministic, N: Normal.

Variable	Meaning	Dist.	Expected values	Std. dev.	Char. value
		Weld 1 - Cathodic protection - Detail 'F'			
$\log K_1$	SN curve parameter	N	11.855	0.2	11.455
$\log K_2$	SN curve parameter	N	15.491	0.2	15.091
m_1	SN curve parameter	D	3		3
m_2	SN curve parameter	D	5		5
		Weld 1 - Free corrosion - Detail 'F'			
$\log K_1$	SN curve parameter	N	16.778	0.2	11.378
$\log K_2$	–	–	–		–
m_1	SN curve parameter	D	3		3
m_2	–	–	–		–

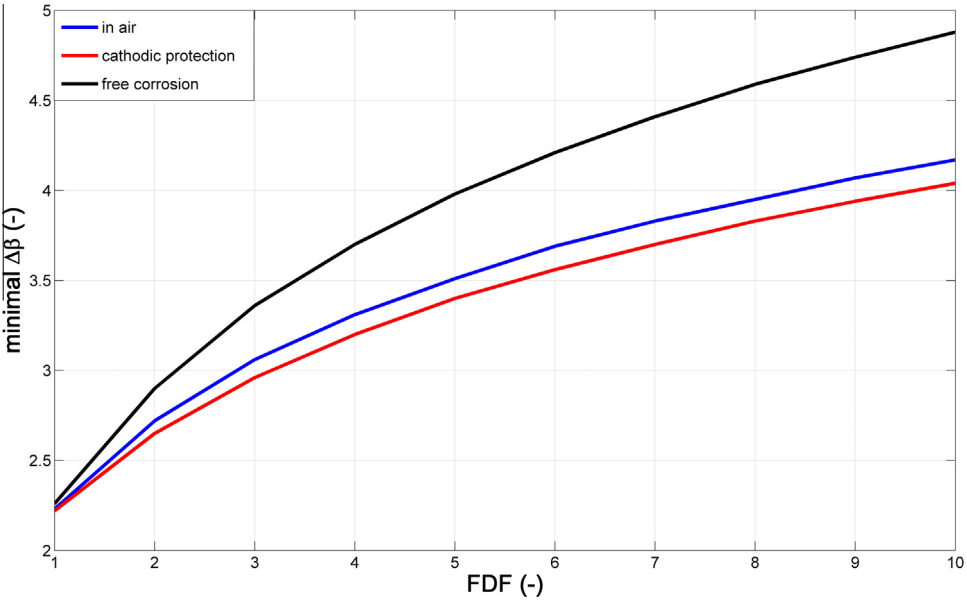

Fig. 7. Minimal annual reliability index of Weld 1 as function of *FDF* for life-time equal to 20 years, $COV_{SCF} = 0.1$ and P-control system using three different SN-curves.

$$D_{rel} = \frac{D_{m=3}}{D_{m=3} + D_{m=5}} \tag{26}$$

where $D_{m=3}$ is the fatigue damage fraction belonging to the SN-curve with m equal to 3 and $D_{m=5}$ the fatigue damage fraction for the part where the SN-curve has parameter m equal to 5. The value D_{rel} is calculated for the conditions at the β-point. For large D_{rel} values, the consideration of the SN-curve with m equals to 5 is of minor importance.

Table 22 shows the relative fatigue damage ratio for different minimal annual and cumulative reliability indices for different SN-curves and control systems. The value of D_{rel} is equal to 1 for SN-curve 'free corrosion' due to the fact that it is a linear SN-curve. Both bilinear SN-curves show that the fraction with $m = 5$ has large impact on fatigue damage. Differences in D_{rel} values for a given reliability level and control system mainly occurs due to the fact that different N_D values (see Eq. (4)) are used.

Table 21
Required *FDF* values for minimal annual reliability index $\Delta\beta$ and minimal cumulative reliability index β at Weld 1 using three different SN-curves. The two different control systems are considered and $COV_{SCF} = 0.1$.

Control system	$\Delta\beta$	Different SN-curves		
		'In air'	'Cathodic protection'	'Free corrosion'
P	3.1	3.2	3.6	2.4
	3.7	6.1	7.1	4.1
PI	3.1	3.3	4.0	2.6
	3.7	6.5	8.0	4.3
Control system	β	Different SN-curves		
		'In air'	'Cathodic protection'	'Free corrosion'
P	2.5	3.1	3.6	2.3
	3.1	5.3	6.1	3.5
PI	2.5	3.1	4.0	2.4
	3.1	5.5	6.8	3.7

Table 22
Fatigue damage ratio D_{rel} values for minimal annual reliability index $\Delta\beta$ and minimal annual cumulative reliability index β at Weld 1 using three different SN-curves. The two different control systems are considered and $COV_{SCF} = 0.1$.

Control system	$\Delta\beta$	Different SN-curves		
		'In air'	'Cathodic protection'	'Free corrosion'
P	3.1	0.25	0.07	1.00
	3.7	0.14	0.02	1.00
PI	3.1	0.47	0.05	1.00
	3.7	0.40	0.04	1.00
Control system	β	Different SN-curves		
		'In air'	'Cathodic protection'	'Free corrosion'
P	2.5	0.33	0.06	1.00
	3.1	0.33	0.04	1.00
PI	2.5	0.33	0.05	1.00
	3.1	0.23	0.04	1.00

5.3. Required FDF with inspections

In order to maintain a certain safety level of the structure, inspections can be performed. Fracture mechanics (FM) are used to model fatigue of welded details due to crack propagation. It is assumed that the crack can be modelled by a semi-elliptical crack and the FM model is calibrated based on the SN-approach described in Section 5.2. Therefore, the parameters $\mu_{\ln C}$ (expected value of $\ln(C)$) and μ_m (expected value of m) are fitted such that the difference between the probability distribution functions for the fatigue life determined by the SN-approach and the fracture mechanical method (considering no inspections) is minimized. Fig. 8 shows an example of the cumulative reliability indices resulting from the SN-curve using a *FDF* value equal to 4 and the calibrated (fitted) fracture mechanics approach. In the following calibrations, results using the PI control algorithm are considered.

Further, X_{SCF} is Lognormal distributed with mean value = 1 and $COV = 0.1$. The focus here is on Weld 1 with uncertainty X_{Wave} according to a mean value equal to 1 and $COV = 0.1$.

Since it is assumed that fatigue cracks are initiated in welded details, it is assumed that the time needed for crack initiation time is negligible ($N_I = 0$) compared with the crack propagation life N_P. The considered stochastic model for modelling crack evolution in Weld 1 is shown in Table 23. Inspections are performed in equidistant intervals and the following different types of inspection techniques are considered:

- Eddy current inspection technique with P_D curve shown in Table 5.
- Inspection with MPI above water (ground test surface), see Table 5.

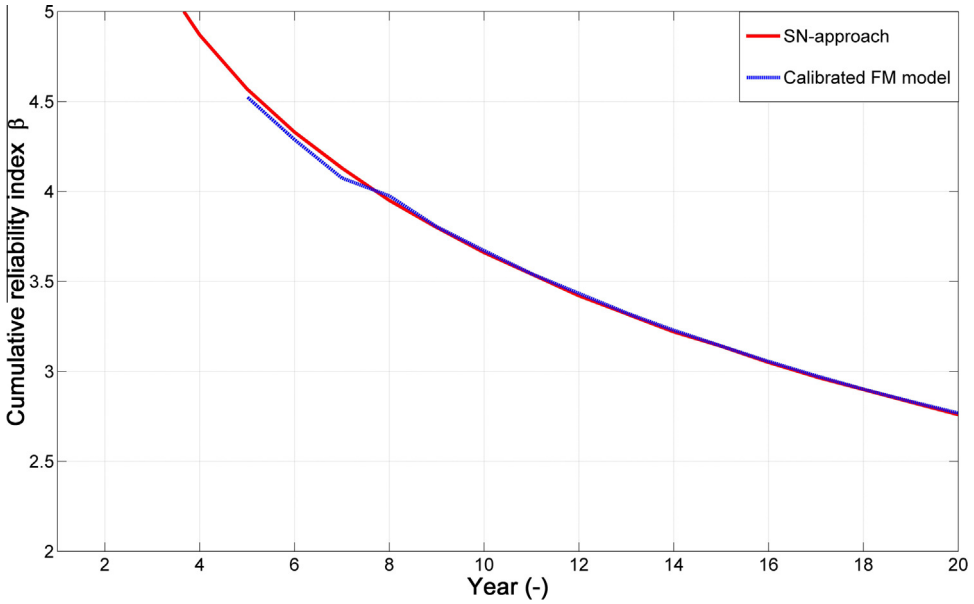

Fig. 8. Example of cumulative reliability indices obtained by SN-approach and the resulting fracture mechanics model. A *FDF* of 4 and a design life-time equal to 20 years is used here. The FM model parameters here are: $\mu_{\ln C} = \ln(29.4)$, $\mu_m = 2.61$.

Table 23
Uncertainty modelling used for fracture mechanical reliability analysis. Std. dev.: Standard deviation, D: Deterministic, N: Normal, LN: Lognormal.

Variable	Meaning	Dist.	Expected values	Std. dev.	Source
a_0	Initial crack	LN	0.2 mm	0.132 mm	[11]
$\ln C$	FM parameter	N	$\mu_{\ln C}$	0.77	[6]
m	FM parameter	D	μ_m		
a_c	Critical crack	D	T (thickness)		
Y	Geometry function	LN	1	0.1	[6]
T	Thickness	D	25 mm		

- Visual inspections with an exponential P_D curve (see Eq. (11)) and smallest detectable crack lengths λ equal to 50 mm and 10 mm.

Furthermore, it is assumed that the crack-depth ratio ($a/2c$) is constant and equal to 0.2. The fracture mechanics approach is based on Monte Carlo Simulations simulating 10^6 life-times for a certain number of inspections per life-time and a certain *FDF* value. The limit state function is based on crack-depth evolution over time (see Eq. (22)).

The results in Table 24 shows the required *FDF* values for a given minimal cumulative and annual reliability index and different inspection methods for a given time interval between inspections. The needed *FDF* values can be decreased when inspections are performed. The more inspections are performed during life-time, the more the *FDF* value can be reduced compared to when no inspections are preformed. When inspections are performed annually, the *FDF* value can be reduced to 1 except for visual inspections with a minimal expected detectable crack size of 50 mm. Largest reductions for a given target reliability level and a number of inspections, can be reached by using the MPI strategy.

For WEC operators not only the required structural safety value for a given number of inspections is of importance but an overall cost tradeoff of including inspections will drive the decision which inspection interval will be chosen.

Table 24
Resulting *FDF* values for minimal annual reliability index $\Delta\beta$ and minimal cumulative reliability index β at Weld 1 for different inspection strategies as well as different numbers of inspections with a constant time interval during life-time. The PI control system is used and $COV_{SCF} = 0.1$.

Inspection strategy	$\Delta\beta$	Time interval (years)						
		20	10	5	4	3	2	1
		Number of inspections						
		0	1	3	4	6	9	19
Eddy current	3.1	3.3	2.6	2.0	1.6	1.3	1.0	1.0
	3.7	6.5	6.4	5.8	5.2	3.7	2.6	1.0
Visual (50 mm)	3.1	3.3	2.6	2.4	2.3	1.8	1.5	1.0
	3.7	6.5	6.5	6.2	6.0	5.1	4.8	2.2
Visual (10 mm)	3.1	3.3	2.4	1.6	1.4	1.1	1.0	1.0
	3.7	6.5	6.2	4.7	4.0	3.1	1.9	1.0
MPI	3.1	3.3	2.3	1.5	1.3	1.0	1.0	1.0
	3.7	6.5	6.1	4.0	3.3	2.8	1.9	1.0
Inspection strategy	β	Time interval (years)						
		20	10	5	4	3	2	1
		Number of inspections						
		0	1	3	4	6	9	19
Eddy current	2.5	3.1	2.9	2.2	1.9	1.5	1.0	1.0
	3.1	5.5	5.2	4.3	3.8	3.0	2.1	1.0
Visual (50 mm)	2.5	3.1	3.0	2.7	2.5	2.1	1.7	1.0
	3.1	5.5	5.4	4.9	4.7	4.1	3.5	1.4
Visual (10 mm)	2.5	3.1	2.7	1.8	1.4	1.1	1.0	1.0
	3.1	5.5	5.0	3.6	3.0	2.2	1.4	1.0
MPI	2.5	3.1	2.5	1.6	1.3	1.0	1.0	1.0
	3.1	5.5	4.7	3.2	2.7	2.1	1.4	1.0

6. Conclusion

Reliability-based calibration of fatigue design factors (*FDF*) is performed in this paper with focus on welded and bolted connections of an offshore bottom-fixed wave energy converter (WEC) with hydraulic floaters. The calibration is based on SN-curves and Palmgren–Miner rule when no inspections of the structural detail is assumed. When inspections are included, a fracture mechanics approach, which is calibrated by the SN-curve approach, is used to model structural fatigue.

FDF values are calibrated for minimal annual reliability indices of 3.1 and 3.7, as well as minimal cumulative reliability indices of 3.1 and 2.5, which are accepted for offshore wind turbines.

The calibration is performed considering the Wavestar device, which is placed in Hanstholm (DK). Three different structural details and two different control strategies are considered. The loads on the structure are calculated based on a hydrodynamic model, which is validated using laboratory experiments. The resulting *FDF* is influenced by the level of uncertainty, which depends on the level of complexity of the considered detail as well as the used load modelling tools. The different control systems and their different model uncertainties have minor effect on the required *FDF* values. Large impact on required *FDF* values has the target reliability level. Smaller target reliability levels lead to smaller required *FDF* values. Furthermore, different environmental conditions, which are represented by different SN-curves affect the required *FDF* values.

When considering annual inspection actions in order to maintain a given safety target level, the required *FDF* values can be reduced from around 6 (without inspections) to roughly 1. The number of inspections leading to the lowest overall costs are driven by economic decision theory and not by minimizing the required *FDF* value. Many inspections most probably increase the operation and maintenance expenses and smaller required *FDF* values decrease the initial investment costs due to less material needed compared when no inspections are performed. The resulting *FDF* values from

the example are in the range proposed by [17] for floating OWTs. *FDF* value requirements for bottom-fixed wind turbines [16] as well as suggestions for WECs from [15] are too low for the shown example. Wave loads assessments tend to have larger modelling uncertainties than wind load assessments. Therefore, for structural details where wave load assessments become important (floating OWTs) and impact the dynamics of the overall system or wave loads are dominating (WECs), the required *FDF* values are larger compared with systems where wind loads are dominating.

The results presented in this paper focus on one WEC concept. For different WEC devices, the load modelling uncertainty will be different due to different load calculation methods as well as different operating conditions (e.g. different working fluids or different wave states when the device is in production mode). Furthermore, the *FDF* value calibration approach is site dependent due to the fact that it includes uncertainties related with the limited wave and wind data as well as different wave and wind directions. The *FDF* calibration results presented in this paper are valid for welded and bolted structures on a floater with a hydraulic cycle as power take-off system at a site where more than two years of wave data is available and only one incoming wave direction is considered. Due to diversity of WECs, more examples should be considered before implementing the results in standards.

Acknowledgements

The authors wish to thank the financial support from the Danish Council for Strategic Research (Contract 09-67257, Structural Design of Wave Energy Devices) which made this work possible.

References

[1] ASM International, Basic understanding of weld corrosion, Am. Soc. Met. (2006).
[2] T. Moan, Reliability-based management of inspection, maintenance and repair of offshore structures, Struct. Infrastruct. Eng. 1 (1) (2005) 33–62, http://dx.doi.org/10.1080/15732470412331289314.
[3] J.D. Sørensen, N. Tarp-Johansen, Reliability-based optimization and optimal reliability level of offshore wind turbines, Int. J. Offshore Polar Eng. 15 (2) (2005) 141–146.
[4] DNV-RP-C203, Fatigue design of offshore steel structures, Det Norske Veritas, 2010.
[5] EN 1993-1-9, Eurocode 3: Design of steel structures - Part 1-9: Fatigue, European Standard, European Committee for Standardization, 2005.
[6] J.D. Sørensen, G. Ersdal, Safety and inspection planning of older installations, J. Risk Reliab. 222 (3) (2008) 403–417, http://dx.doi.org/10.1243/1748006XJRR136.
[7] F. Ferri, S. Ambühl, B. Fischer, J.P. Kofoed, Balancing power output and structural fatigue of wave energy converters by means of control strategies, Energies 7 (4) (2014) 2246–2273, http://dx.doi.org/10.3390/en7042246. URL <http://www.mdpi.com/1996-1073/7/4/2246>.
[8] H.O. Madsen, S. Krenk, N.C. Lind, Methods of Structural Safety, second ed., Dover Publications, Inc., Mineola, NY, USA, 2006.
[9] M. Lemaire, A. Chateauneuf, J.-C. Mitteau, Structural Reliability, ISTE Ltd. (UK) and John Wiley & Sons, Inc, USA, 2009.
[10] ISO 19902, Petroleum and Natural Gas Industries - fixed steel offshore structures, ISO standard, 2005.
[11] JCSS, Probabilistic model code, Joint Committee on Structural Safety, 2001.
[12] J.D. Sørensen, Reliability-based calibration of fatigue safety factors for offshore wind turbines, in: International Offshore and Polar Engineering Conference Proceedings (2011) 463–470.
[13] S. Marquez-Dominguez, J.D. Sørensen, Fatigue reliability and calibration of fatigue design factors for offshore wind turbines, Energies 5 (6) (2012) 1816–1834, http://dx.doi.org/10.3390/en5061816.
[14] ISO 2394:1998, General principle on reliability for structures, ISO Standard (1998).
[15] DNV/Carbon Trust, Guidelines in design and operation of wave energy converters, Det Norske Veritas, 2005.
[16] DNV-OS-J101, Design of offshore wind turbine structures, Det Norske Veritas, 2013.
[17] DNV-OS-J103, Design of floating wind turbine structures, Det Norske Veritas, 2013.
[18] S. Ambühl, M. Kramer, J.D. Sørensen, Reliability-based structural optimization of wave energy converters, Energies 7 (12) (2014) 8178–8200, http://dx.doi.org/10.3390/en7128178. URL <http://www.mdpi.com/1996-1073/7/12/8178>.
[19] IEC 61400-1, Wind turbines - part 1: design requirements for offshore wind turbines, International Electrotechnical Comission, 2009.
[20] DNV-OS-J101, Design of offshore wind turbine structures, Det Norske Veritas, 2011.
[21] GL, Guideline for offshore certification of offshore wind turbines, Germanischer Lloyd Wind Energie GmbH, Wind Energy Comittee, Hamburg, Germany, 2005.
[22] ASTM Standard E 1049-1085, ASTM standard for cycle counting fatigue analysis, 2005.
[23] J.D. Sørensen, Framework for risk-based planning of operation and maintenance for offshore wind turbines, Wind Energy 12 (5) (2009) 493–506.
[24] DNV 95-2018, Guideline for offshore structural reliability analysis - general, Det Norske Veritas, 1995.
[25] D. Straub, Generic approaches to risk-based inspection planning for steel structures (Ph.D. thesis), ETH Zuerich, Zuerich, Switzerland, 2004.
[26] P.C. Paris, F. Erdogan, A critical analysis of crack propagation laws, J. Basic Eng. 85 (1963) 528–533.
[27] BS 7910, Guide to methods for assessing the acceptability of flaws in metallic structures, Bristish Standard, 2005.

[28] M. Kramer, L. Marquis, P. Frigaard, Performance evaluation of the wavestar prototype, in: 9th European Wave and Tidal Energy Conference (EWTEC), Southampton, UK, 5th–9th September 2011, (2011).
[29] DanWEC, Danish wave energy center, <http://www.danwec.com>.
[30] R. Hansen, M. Kramer, Modelling and control of the wavestar prototype, in: 9th European Wave and Tidal Energy Conference (EWTEC), Southampton, UK, 5th–9th September 2011, (2011).
[31] F. Ferri, M. Kramer, A. Pecher, Validation of a wave-body interaction model by experimental tests, International Offshore and Polar Engineering Conference. Proc. Int. Soc. Offshore Polar Eng. (2013) 500–507.
[32] IEC 61400-1-MT01, Safety Factors - background document, International Electrotechnical Comission, 2013.